

Cloud Types Simulated by the NCEP GFS Model

Y. Luo

*National Institute of Aerospace
Hampton, Virginia*

S. K. Krueger

*University of Utah
Salt Lake City, Utah*

Introduction

Clouds and their interactions with radiation is recognized by the most recent IPCC (Intergovernmental Panel on Climate Change; 2001) report as the greatest uncertainty in future projections of climate, and, despite the considerable improvement of the physical realism of cloud representation in general circulation models, representation of clouds and their feedbacks is still the weakest component of current General circulation models (e.g., Senior and Mitchell 1993, Cess et al. 1996). In the last 5 to 10 years, cloud resolving models (CRMs) and single column models (SCMs) have become extensively used tools in evaluation and improvement of cloud representation in General circulation models (Randall et al. 1996). CRMs, because of their ability to explicitly simulate cloud-scale dynamics and meso-scale processes, are increasingly being used for understanding cloud processes (e.g. Chaboureau and Bechtold 2002, Kohler 1999, Krueger et al. 1995b, c). Recently, a high-resolution CRM has been embedded in a general circulation model to replace most of the physical parameterizations (Grabowski 2001). This multiscale modeling framework approach has been shown to produce the Madden-Julian Oscillation as well as higher-frequency tropical waves in a much more realistic manner than a general circulation model with a traditional cloud parameterization (Khairoutdinov and Randall 2001, Khairoutdinov et al. 2003). However, detailed evaluations of the ability of CRMs to represent the radiative effects of various cloud types have not been made. The usefulness of SCMs to evaluate/develop/improve cloud parameterizations in General circulation models has been improved partly by the increasing use of CRMs, and partly by the availability of more observations suitable for SCM studies produced by projects such as the Atmospheric Radiation Measurement program (ARM; Stokes and Schwartz 1994, Ackerman and Stokes 2003).

Cloud properties for large spatial and temporal domains are now available from geostationary satellite observations with spatial resolution on the order of one to several kilometer(s) using advanced retrieval methods. One example of those datasets is that produced by Patrick Minnis' group at NASA Langley Research Center (LARC). This dataset is used in this study and a description of it will be given in section 3. Another example is the ISCCP (International Satellite Cloud Climatology Project; Rossow and Schiffer 1991 and 1999) DX data, which has a spatial sampling resolution of approximately 30 km and a temporal sampling interval of 3 h (Rossow et al. 1996). These datasets make it possible to evaluate the radiative effects of various cloud types in a CRM or SCM/general circulation model simulation.

Traditionally, evaluations of general circulation model cloudiness compare simulated and observed cloud properties using climatological and often zonal averages (e.g. Weare et al 1996). Averaging in time and/or space can obscure the presence of compensating errors and provide very limited information about the sources of errors. Two new trends in the studies for general circulation model cloudiness evaluation have appeared recently. One trend is an increasing use of the compositing method. This method compares cloud properties as a function of meteorological conditions and thus cloudiness is directly connected to meteorological processes. Jakob (2003) recently proposed a new strategy for cloud parameterization evaluation. The key of the proposed strategy was to link the evaluation of the model climate to the selection of case studies through the use of compositing techniques. Xu et al. (2004) proposed an object classification methodology which classifies the satellite data into cloud systems defined by cloud-system types, sizes, geographic locations, and the matched large-scale environments. They analyzed the probability density functions (PDFs) of the identified cloud objects based upon the pixel-level information and proposed a method which can use these statistical properties to evaluate models. The other trend is more explicit use of cloud-scale (i.e. km-scale) observations. It is being increasingly recognized that the scales resolved by CRMs are the most physically appropriate ones for developing and testing cloud parameterizations and models should be tested against observed cloud-scale statistics, as pointed out by Randall et al. (2003). Such cloud-scale statistics can be obtained from satellite observations, such as International Climatology Program (ISCCP) and Clouds and the Earth's Radiant Energy System (CERES) (Wielicki et al. 1996), from cloud radar observations, such as those obtained at the ARM sites, and from precipitation radar observations, such as those provided by the Tropical Rainfall Measuring Mission (TRMM). Examples of comparing general circulation model results composited by meteorological parameters to cloud-scale data from satellite observation are Klein and Jakob (1999), Tselioudis et al. (2000), and Norris and Weaver (2001).

Using the cirrus property statistics from km-scale observations collected at the ARM Southern Great Plains (SGP) site and the bulk microphysical properties of thin cirrus layers produced by Mace et al. (2001), we demonstrated a new method to evaluate a SCM/general circulation model cloud properties (Luo et al. 2004). We also evaluated the SCM's parameterizations for convective detrainment and microphysical processes through comparison with a CRM and related the errors of the SCM's cirrus properties to the defects in its parameterizations (Luo and Krueger 2004). These constitute the Part I and II of our papers. The SCM used in our study as an example to demonstrate our method is based on the National Centers of Environmental Prediction (NCEP) Global Forecast System (GFS) atmospheric model and the CRM used is the UCLA/CSU CRM. In this paper (Part III), we assess radiative effects of various cloud types, defined by cloud top pressure and cloud optical depth, simulated by the SCM as well as by the CRM, using pixel-level satellite retrievals.

Using the profiles of cloud fraction and cloud water/ice mixing ratio from the SCM simulation and the km-scale cloud fields from the CRM simulation as inputs to the ISCCP cloud-simulator and a radiative transfer scheme, we diagnosed the occurrence frequencies and radiative effects of various cloud types. Model's errors are estimated through a comparison with the kmscale satellite observations. Possible sources of the errors are related to the distributions of cloud optical depth and top pressure/temperature, as well as the occurrence frequency and timing of cloud type. Our first objective is to demonstrate an evaluation method that gives more insights to the ability of models (CRM and SCM/general circulation model) in simulating clouds. The second goal of this study is to evaluate the performance of the two

models used. Section 2 includes a simple description of the simulations made using the two models. Section 3 describes the observational dataset used. The analysis methods are presented in section 4. The cloud radiative forcings (CRFs) by various cloud types and their occurrence frequencies simulated by the two models are compared with the satellite observations in section 5. A summary and discussions of these results are provided in section 6.

2. Simulations

The University of California-Los Angeles/Colorado State University (UCLA/CSU) CRM and a SCM version of the NCEP GFS atmospheric model are used in this study. The large-scale forcing data from the ARM variational analysis (Zhang and Lin 1997, Zhang et al. 2001) for the Southern Great Plains (SGP) site summer 1997 Intensive Operation Period (IOP) were used to “drive” the models. The forcing data represent the states of an atmospheric column whose horizontal size is about 100,000 km². The IOP covered 29 days starting from June 23, 1997 23:30 UTC which contained several intensive precipitation events and dry and clear days associated with the activities of the large-scale upper-level troughs and ridges over the North America continent. Clouds were observed by the Geostationary Operational Environmental Satellite (GOES) to be mainly with high-tops during the IOP (Figure 1). The occurrence frequency of cirrus clouds simulated by the CRM and the SCM, respectively, is correlated better with the satellite observations during the 14-day subperiods A, B, and C (defined in Figure 1) than the other subperiods of the IOP (Luo et al. 2003, 2004). The major reason is the relatively smaller large-scale advection of hydrometeor into or out of the SGP domain during these ABC subperiods. Profiles of the large-scale advection of hydrometeor were not quantitatively available and not used in the simulations. However, the animation of GOES infrared (IR) imagery does reveal that there were relatively less cloud systems moved in or out of the SGP domain during the 14-day subperiods. We focus our analysis on these subperiods in this study. More detailed description about the precipitation events during the three subperiods can be found in Xie et al. (2002).

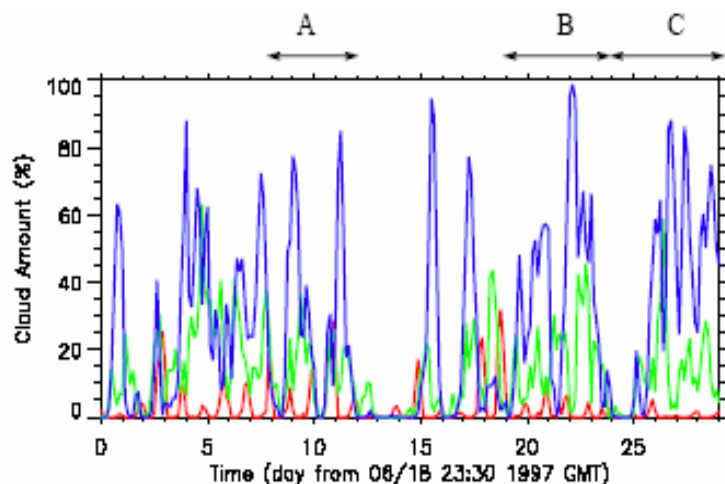


Figure 1. The GOES observed cloud amounts at high-(blue), mid-(green), and low-levels (red) during the summer 1997 SCM IOP at the ARM SGP site. The A, B, and C shown at the top are the

subperiods when large-scale advection of hydrometeors, which was not used in the simulations due to lack of observation, was relatively weak over the SGP site.

The CRM includes two-dimensional anelastic dynamics, three-phase cloud microphysics, a third-moment turbulence closure, and an interactive radiative transfer scheme (Krueger 1988, Krueger et al. 1995a, Xu and Randall 1995). The grid interval used is 2 km in horizontal and varies in vertical from about 100 m near the surface to about 1 km near the model's top (18 km). The CRM was run for the IOP by Kuan-Man Xu at the National Aeronautics and Space Administration (NASA) Langley Research Center (LARC) and details of the CRM simulation can be found in Luo et al. (2003). We used the SCM developed by Shrinivas Moorthi at the NCEP. The SCM is based on the year 2001 version of the NCEP GFS atmospheric model. Description of the model that was implemented operationally on May 15, 2001 is given in Moorthi et al. (2001). The SCM explicitly predicts cloud water or ice mixing ratio and diagnoses stratiform cloud fraction from the cloud condensate mixing ratio and relative humidity. The deep convection parameterization is a simplified Arakawa-Schubert (1974) scheme with only one cloud type considered (Pan and Wu, 1995). The effects of convective cloud are neglected in radiation calculation. More details of the SCM configuration were provided in Luo et al. (2004).

3. Observations

Satellite observations we used include both the longwave (LW) radiative flux and shortwave (SW) albedo at the top of the atmosphere (TOA) from GOES-8 and cloud products generated by Patrick Minnis' group at NASA LARC. The LW broadband flux was derived by conversion from narrowband LW radiance. The monthly mean uncertainty (rms error) of the area-averaged outgoing longwave radiation (OLR) is about 10 Wm^{-2} over the SGP variational analysis domain (Khayer et al. 2002). We calculated the reflected shortwave (SW) flux from broadband albedo, whose monthly mean uncertainty (rms error) is about 0.02 over the SGP SCM analysis domain based on the results from Khayer et al. (2002).

Briefly, Minnis' group uses a general approach for quantifying clouds, which consists of two stages: cloud identification and cloud properties retrieval. Cloud is identified by comparing an observed radiance or set of radiances at different wavelengths to the values expected from a clear (cloudless) scene (pixel). If the observed radiance is sufficiently different from the clear-sky value, the pixel is designated as cloudy. For each cloudy pixel, variables including cloud phase, cloud top temperature, cloud optical depth, effective droplet radius (r_e) or effective ice crystal diameter (D_e), and liquid water path (LWP) or ice water path (IWP) are determined iteratively by matching the observed radiances with results from radiative transfer models and cloud microphysical models for a wide range of particle sizes and cloud and clear-sky temperatures. The profiles of temperature and humidity from the Rapid Update Cycle (RUC) 3-hourly soundings are used by the Minnis group in their retrieval. The geostationary satellite cloud products include cloud information over a large spatial domain at 4-km space resolution and at half-hour time intervals for all cloud types, so that occurrences, properties, radiative effects, and spatial distributions of various cloud types can be analyzed. Their disadvantages include the varying reliability of the retrievals. One source of uncertainties in satellite retrievals is the assumptions made about the cloud, atmosphere, and surface characteristics. The most important assumptions include: (a) Cloud optical properties are uniform over the image pixels; hence, cloud cover of pixel is either zero or

one. (b) Clouds are single layers. (c) Surface and atmospheric optical properties are uniform over the image pixels.

Minnis' group used a pair of multi-spectral algorithms, the Visible-Infrared-Solar-Infrared-Split Window Technique (VISST) for daytime and Solar-Infrared-Station (SIRS) method 8 for nighttime, as described by Minnis et al. (1995) using the models of Minnis et al. (1998), together with the technique of Minnis and Smith (1998) to analyze the half-hourly, 4-km GOES-8 imager data [0.65 μm , visible (VIS); 3.9 μm , solar-infrared (SIR); 10.8 μm , IR; and 12.0 μm , split-window (SWC)]. To compare, ISCCP retrieval used a VIS-IR bispectral method in daytime and an IR-only method in nighttime so that cloud optical properties could not be retrieved for nighttime. The Minnis multispectral algorithms use radiances in two more channels than ISCCP: the SIR radiance to estimate cloud particle size and the SWC radiance to help determine cloud phase (Young et al. 1997). The ISCCP DX data also provide cloud properties at pixel-level horizontal resolution (i.e. km-scale). However, the cloud products are available during daytime only, and were sampled every 30 km and 3 hr. Over the SGP variational analysis domain, there are only about 75 pixels every 3 hr in daytime. By comparison, the Minnis pixel-level cloud products have about 7000 pixels every half hr. For our study --evaluating the CRFs and occurrence frequencies of various cloud types in 29-day simulations, the Minnis cloud products are more appropriate because of a much larger number of samples than the ISCCP DX dataset.

4. Analysis Method

We analyzed the occurrence frequencies and CRFs of various cloud types using the satellite data and results from the two simulations. Before describing our methods, the definition of the cloud types is presented here. We define the cloud types using cloud optical depth and cloud-top pressure following the ISCCP definitions. We group the clouds into 8 types (Figure 2): 4 high-top types: very thin (τ : 0.1 - 1.3), thin (τ : 1.3 - 3.6), moderate (τ : 3.6 - 9.4), and thick (τ > 9.4), 2 middle-top and 2 low-top types: thin (τ : 0.1 - 9.4) and thick (τ > 9.4). High-level is defined as above 440 mb level, low-level is defined as below 680 mb, and mid-level is in between. We combine clouds with τ greater than 9.4 into one cloud type at each level because the satellite cloud-property retrieval method used by Minnis' group for nighttime can not accurately derive the values of τ greater than 10. Clouds with τ less than 0.1 are excluded because most of them are difficult to detect by the satellite retrieval at any time. Clouds are grouped into 4 types at the high-level and 2 at the mid- and low-levels because most clouds during the IOP were high-top clouds as observed by the satellite (and the cloud radar at the SGP site). Note that the cloud names used in Figure 2 and hereafter are for convenience; they are different from conventional definitions of optically "thin," "moderate," and "thick" clouds. Our studies of cirrus occurrence (Luo et al. 2003, 2004) indicate better performance of the CRM/SCM simulation during the 14-day ABC subperiods (Figure 1) when the large-scale advection of hydrometeors was relatively small, so we focus our analysis on the same subperiods in this study.

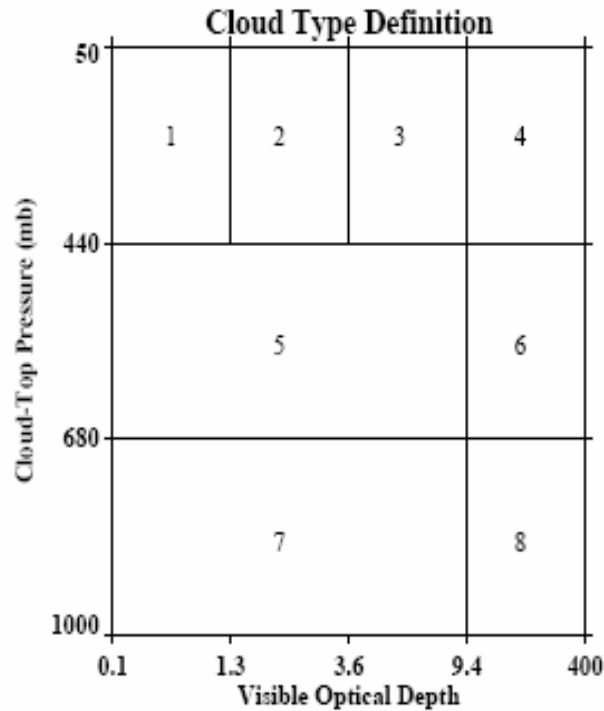


Figure 2. The definition of the eight cloud types used in the study.

4.1 Occurrence Frequency of Cloud Types

A. Satellite data

Based on the Minnis half-hourly pixel-level cloud products, including cloud phase, cloud-top pressure, and cloud visible optical depth, we calculated the occurrence frequencies of various cloud types, as defined by the total cloud visible optical depth and the cloud-top pressure of the highest cloud layer (Figure 2), at mostly half-hour intervals. The occurrence frequency of a cloud type is the fraction of the total number of pixels occupied by the cloud type within the SGP SCM analysis domain.

B. SCM and CRM

We deployed the “ISCCP simulator” to determine the cloud type frequency for the CRM and SCM simulations in order to get the results from the models that are comparable to the satellite observations. The ISCCP simulator was developed by S. Klein (GFDL) and M. Webb (UKMO) to provide a connection between results from a general circulation model/SCM and cloud types defined by satellite-observed visible and IR radiances. The inputs to the ISCCP simulator include general circulation model/SCM simulated profiles of temperature, pressure, cloud water/ice mixing ratio, cloud fraction (defined as the horizontal area of each grid box covered by clouds), $0.67 \mu\text{m}$ cloud optical depth, $10.5 \mu\text{m}$ cloud emissivity, and surface skin temperature (T_s) and $10.5 \mu\text{m}$ emissivity of the surface. All inputs are general circulation model/SCM grid-mean values except for the cloud optical depth and cloud emissivity

which are in-cloud values. Firstly, the ISCCP simulator distributes the general circulation model/SCM predicted grid-mean cloud water/ice content at each level into a number of subgrid columns using the profile of the cloud fraction together with a cloud overlap assumption, neglecting the cloud horizontal inhomogeneity at a level. Secondly, for each subgrid column, the IR radiance at the TOA is calculated, including emission/absorption of the surface, water vapor, and clouds at all levels. Thirdly, the cloud-top temperature (T_c) is computed for each subgrid column from the emissivity-adjusted IR radiance and the cloud-top pressure is determined as the model level with the same atmospheric temperature as T_c . The occurrence frequencies of cloud types as defined by cloud visible optical depth and cloud-top pressure are then determined.

We calculated the T_s from the downward (F_{dn}) and upward (F_{up}) LW flux measurements by Solar and Infrared Observation Stations (SIROS) distributed over the SGP site using the following formula, assuming that the surface emissivity (ϵ) is 0.98:

$$T_s = \left(\frac{F_{up} - (1 - \epsilon)F_{dn}}{\epsilon\sigma} \right)^{1/4} \quad (1)$$

where σ is the Stefan-Boltzmann constant. The subgrid-scale horizontal inhomogeneity of the SCM clouds was neglected as in the NCEP GFS atmospheric model. Therefore, at a cloudy model level, the in-cloud value of water/ice mixing ratio is the grid-mean value divided by the SCM predicted cloud fraction. The in-cloud water/ice mixing ratio and specified effective sizes of cloud water droplets/ice crystals were used to diagnose cloud optical properties using parameterization of Fu and Liou (1993) for ice clouds and of Hu and Stamnes (1993) for liquid clouds. The effective radius of cloud droplets/ice crystals were determined by the SCM temperature in the same way that the NCEP GFS model did. The occurrence frequencies of cloud types were diagnosed at 15-min intervals.

Unlike a general circulation model/SCM, a CRM explicitly simulates 2-D or 3-D cloud fields, so no overlap assumption is needed to get a km-scale cloud distribution. We modified the original ISCCP simulator for use in our CRM analysis. Each CRM grid column is considered as a satellite pixel. The cloud optical depth and IR emissivity are diagnosed directly from the CRM simulated profiles of cloud fields and atmospheric state for each column using the schemes of Hu and Stamnes (1993) and Fu and Liou (1993). The cloud droplet effective radius is specified as 10 μm . Both cloud ice and snow are treated as ice-phase clouds with specified effective diameters: 50 μm for cloud ice and 150 μm for snow. For mixed phase clouds, the visible optical depths of the liquid water droplets and ice crystals were added to obtain the total visible optical depth, while the absorption coefficients of the cloud droplets and ice crystals were added to obtain the total cloud absorption coefficient used for calculating the IR emissivity. We determined the occurrence frequencies for the cloud types in the CRM simulation every 5 min. Cloud type occurrence frequency is defined as the fraction of model columns that contain each cloud type.

The specified equivalent diameters for cloud ice crystals used in the CRM radiation calculation are uncertain. They are based on retrievals for thin cirrus (Mace et al. 2001). Using smaller diameters could change cloud type amounts, e.g., increase thick high-top cloud amount (type 4). More accurate

values from observations are desired. It would be useful to quantify the uncertainty in the CRM results caused by the uncertainty in specified droplet/crystal size.

4.2 Cloud Radiative Forcing

The “cloud radiative forcing” (CRF) is defined to be the difference between the radiative flux absorbed under all-sky and clear-sky conditions

$$CRF = (OSR_{clr} - OSR) + (OLR_{clr} - OLR) \quad (2)$$

where OSR is outgoing (reflected) solar radiation, and OLR is outgoing longwave radiation, the suffix “clr” indicates the clear sky fluxes and no suffix refers to all-sky fluxes. The first and second parts of the right-hand-side of Eq. (2) are, respectively, the negative shortwave CRF and positive longwave CRF. By definition, the CRF measures the effect of clouds on radiation budget.

A. Satellite observation

Using half-hourly Minnis pixel-level data, we averaged the TOA LW flux and SW albedo over the pixels that are within SGP variational analysis domain and either detected as clear or cloudy with a reliable cloud property retrieval, to get the area-averaged LW flux and SW albedo for all-sky, clear-sky, and each of the eight cloud types. During twilight, the SGP variational analysis domain is partly sunlit and SW albedo is averaged over sunlit pixels only. The fractional areas for clear sky and for each of the eight cloud types are also computed. We then linearly interpolated the area-averaged quantities in time to get TOA LW fluxes, SW albedos, and the fractional areas for all-sky, clear-sky, and cloudy-sky at one-hour intervals. Since the clear-sky area-averaged LW flux and SW albedo are needed for the CRF calculations at each hour, the values at the two available times closest to the interpolated time were used for interpolation. The hourly averaged SW upward flux (OSR) was calculated from the SW albedo (α), using

$$OSR = \alpha s \quad (3)$$

where s is the solar insolation. We used the following formula to calculate s :

$$s = S \times \left(\frac{d_m}{d} \right)^2 \times \cos(\theta) \quad (4)$$

where S (1366 Wm^{-2}) is the solar constant at the mean sun-earth distance (d_m), d is the instantaneous sun-earth distance, θ is the hourly averaged solar zenith angle. For each hour of the IOP, the values of $\cos(\theta)$ and $\frac{d_m}{d}$ at the SGP Central Facility (CF; latitude 36.61°N , longitude 97.49°W) were computed by integrating over six evenly-spaced time intervals, i.e., each time interval is 10 min.

B. SCM and CRM

We diagnosed the LW and SW fluxes at the TOA from the cloud and atmospheric profiles simulated by the CRM and the SCM using the radiative transfer (RT) model developed by Fu and Liou (1992, 1993). This broadband radiation scheme integrates the δ -four stream model for radiative transfer in nonhomogeneous atmosphere, the correlated κ -distribution method to account for nongray gaseous absorption, and the scattering and absorption properties of spherical liquid droplets and nonspherical ice crystals in 6 shortwave (0.2 -4.0 μm) and 12 longwave (2200 - 1cm^{-1}) bands. The model includes absorption due to H_2O , CO_2 , O_3 , N_2O , and CH_4 in the LW and by H_2O , CO_2 , O_3 , and O_2 in the SW. For liquid-water clouds, a parameterization for the single-scattering properties is based on Mie calculations with a mean effective radius to account for the cloud droplets size distribution for radiative calculations. The single-scattering properties of non-spherical ice crystals are considered with an equivalent ice diameter and ice mixing ratio as inputs. The required inputs to the RT model include the surface SW spectral albedos, the surface IR spectral emissivities, and the surface skin temperature, as well as the profiles of hydrometeor mixing ratios predicted by the models and the specified effective sizes for cloud droplets and ice crystals. The effective sizes are specified the same way as described in section 4.1. The time interval is 5-min for the CRM and 1-hr for the SCM. Note that the RT calculation was performed for each of the SCM subgrid columns determined by the ISCCP simulator.

The 3 hr SGP domain-averages of the broadband downward (F_{dn}) and upward (F_{up}) LW fluxes at the surface measured by the SIROs were used to diagnose the broadband albedo (α). We linearly fit the α as a function of $\cos(\theta)$ (where θ is the solar zenith angle) and used the α to obtain the spectral albedos which are $c_i\alpha$, with $c_i = (0.428, 1.507, 1.542)$ for wavelength intervals of (0.2 -0.7, 0.7 -1.3, 1.3 -4.0) μm , respectively. This corresponds to a surface that is 80% grass and 20% shrub (Q. Fu 2003, personal communication). The 3 hr T_s calculated using Eq. (1), which represents a CRM/SCM domain-average, was interpolated to get values at 5 min intervals for the CRM and 1 hr for the SCM. At each time the same value of T_s was used for all of the CRM grid/SCM subgrid columns.

The TOA LW and SW all-sky fluxes are simply the fluxes averaged over the entire CRM/ SCM domain. To get the TOA clear-sky fluxes, we averaged the fluxes at the columns which were clear or contained cloud with τ less than 0.1. Including clouds with τ less than 0.1 in the clear-sky fluxes calculation is reasonable since most of these optically thin clouds were missed by the satellite retrievals. The cloud amount and TOA fluxes from each of the eight cloud types were also determined for each time. We computed the overcast LW and SW CRFs as well as the LW, SW, and net CRFs for each cloud type in the same way as for the Minnis data.

5. Results

5.1 Cloud Radiative Forcing

We provide the net, LW, and SW CRFs by all clouds averaged over the 14-day subperiods A, B, and C from the satellite observation and the two simulations in Table 1. The net CRF by all clouds during the ABC subperiods is -5 Wm^{-2} (Minnis), 0 Wm^{-2} (CRM), and 4 Wm^{-2} (SCM), respectively. The LW CRF estimated from the satellite observations is 38 Wm^{-2} , greater than that from the CRM (31 Wm^{-2}) and the

SCM (30 Wm^{-2}). The SW cooling effects of clouds in the two simulations (-31 and -26 Wm^{-2} for the CRM and the SCM, respectively) were weaker than those observed (-43 Wm^{-2}). This comparison is equivalent to the traditional method used to evaluate general circulation model climate: comparing the monthly averaged TOA fluxes and/or CRFs from General circulation models with observations. The numbers like those shown in Table 1 are ‘net’ results for all cloud types. It is very likely that some cloud types are represented better than other cloud types in a model. It is also possible that one cloud type causes errors in CRFs which are opposite in sign to the errors due to other clouds. One cannot tell from such a comparison which cloud types are the major contributors to the model’s errors in CRFs and hence cannot get much useful guidance for model improvement.

Table 1. Cloud radiative forcings (W/m^2) averaged over the 14-day subperiods A, B, and C from the Minnis data, the CRM and SCM simulations.

	LW CRF	SW CRF	Net CRF
Minnis	38	-43	-5
CRM	31	-31	0
SCM	30	-26	4

Figure 3 presents a comparison among the observation and the two simulations of the net CRFs of the eight cloud types. The CRM results are closer to the satellite observations than the SCM results for most cloud types except for the optically thin high-top clouds (type 2), for which the observational net CRF is between the two models’ results. Both the observation and the CRM results show that optically thin ($\tau < 9.4$) high-top clouds (types 1, 2, 3) had a warming effect and all other cloud types had a cooling effect. The CRM cloud types had weaker effects than those observed with about $\pm 1 \text{ Wm}^{-2}$ differences except for type 4 (about $+5 \text{ Wm}^{-2}$). A few weaknesses of the SCM results can be found from Figure 3. One is that the thick high-top clouds (type 4) had a warming effect, as opposed to the satellite observation and the CRM results which show cloud type 4 had the largest cooling effect among all cloud types. Another weakness in the SCM simulation is that the thin low-top clouds (type 7) had more cooling effect (7 Wm^{-2}) than the satellite observation (2.5 Wm^{-2}) and the CRM result (0.5 Wm^{-2}). Third, very few thick middle-top clouds (type 6) and no thick low-top clouds (type 8) were simulated by the SCM so that their CRFs were zero. According to the satellite observation and the CRM, those clouds had a 2 or 1 Wm^{-2} cooling effect.

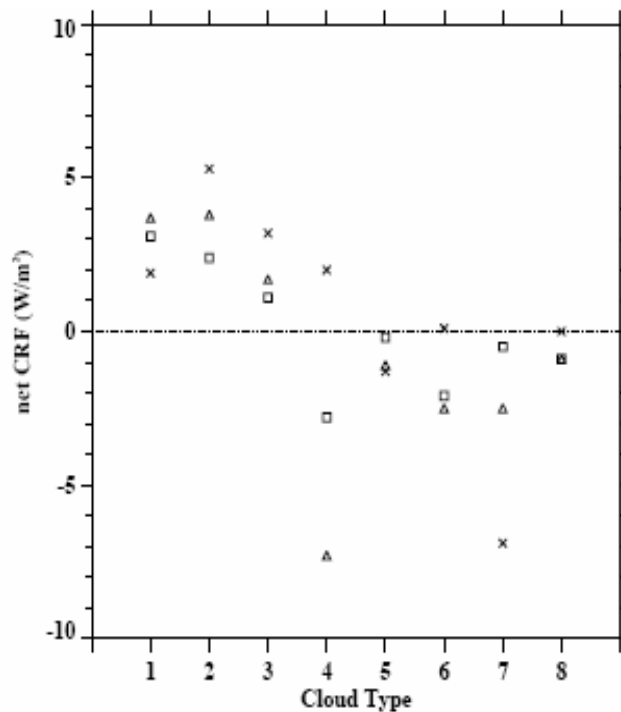


Figure 3. The net CRFs of the eight cloud types from the satellite observation (triangles), the CRM (squares) and the SCM (crosses) simulations during the 14-day subperiods A, B, and C.

The net CRFs are determined by the sum of LW and SW CRFs. The occurrence frequency and times when clouds present influence both LW and SW CRFs. In addition, LW CRF is mainly determined by the effective radiating temperature difference between the cloud and the surface while cloud optical depth is the most important factor determining SW CRF. Errors in LW CRF may indicate defects in the temperatures (vertical locations) of cloud layers while errors in SW CRF may be more related to the representation of cloud microphysical processes. Figure 4 shows the LW CRFs of the eight cloud types from the satellite data and the two simulations. The CRM's values are at most 2 Wm^{-2} smaller than the observation. They both show strong warming effects by high-top clouds, particularly the deep convective clouds and closely associated thick anvil clouds (type 4), and negligible warming effects by clouds with middle- and low-tops. Compared to the satellite observation and the CRM result, the SCM cloud type 4 had too little (about one fourth) warming effect and its type 2 (thin high-level clouds) had too much (twice) warming effect. Similar to Figure 4, Figure 5 shows the SW CRFs of the eight cloud types. Obviously, thick high-top clouds were the dominant contributor to the total SW CRF as both the observation and the CRM suggested. Most of the CRM cloud types had lesser cooling effects with about 1 or 2 Wm^{-2} differences from the observation, except for the type 4 the difference was about 7 Wm^{-2} . These differences are within the range of uncertainty of the satellite observation. It is obvious that the SCM cloud type 4 had much weaker cooling effect (1 Wm^{-2}) than the satellite (22 Wm^{-2}) and the CRM (15 Wm^{-2}). The cooling effects of the SCM cloud types 2 and 7 were about 4 Wm^{-2} larger than the satellite.

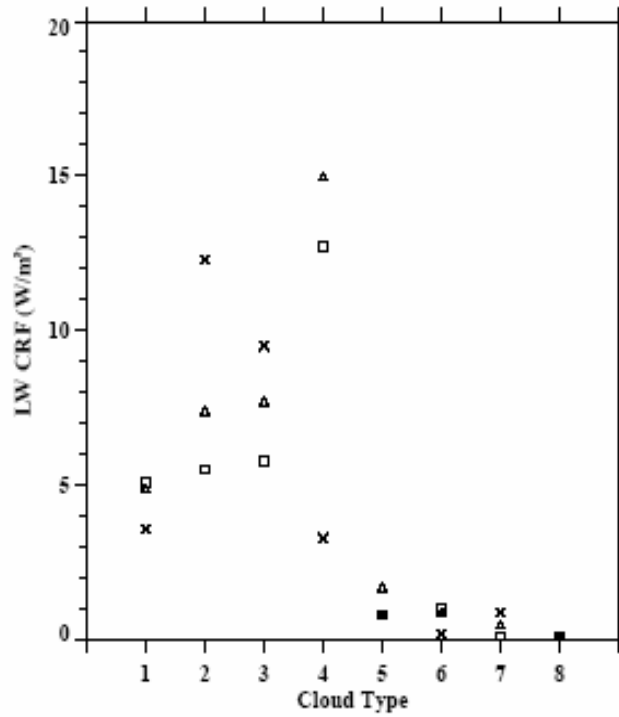


Figure 4. The LW CRFs of the eight cloud types from the satellite observation (triangles), the CRM(squares) and the SCM (crosses) simulations during the 14-day subperiods A, B, and C.

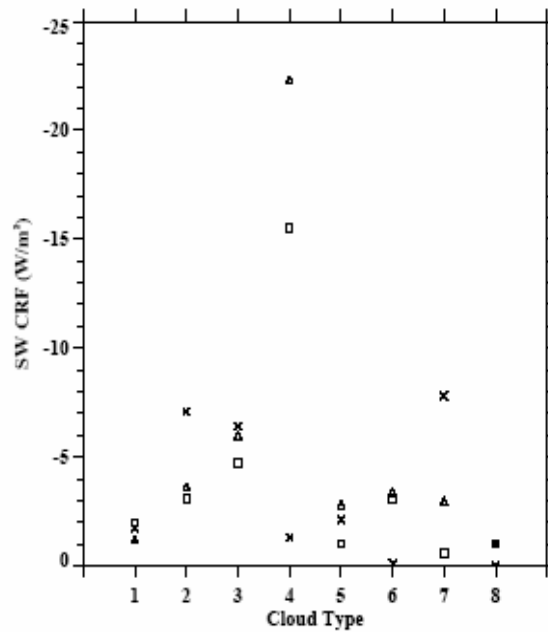


Figure 5. The SW CRFs of the eight cloud types from the satellite observation (triangles), the CRM simulations during (squares) and the SCM (crosses) simulations during the 14-day subperiods A, B, and C.

We conclude that the CRM performed better than the SCM in simulating the radiative effects of various cloud types. The major weakness found in the CRM is that the thick high-top clouds (type 4) had 7 Wm^{-2} lesser SW cooling and 2 Wm^{-2} lesser LW warming than the observation. The SCM seems to have difficulties in simulating correct radiative effects of cloud types 4 (thick high-top clouds), 2 (optically thin high-top clouds), and 7 (optically thin low-top clouds). Compared to the observational results, the SCM's thick high-top clouds had too little LW warming effect and an even smaller SW cooling effect. As a result, the SCM cloud type 4 had a net warming, as opposed to a cooling effect seen in the observations and the CRM. The SCM cloud types 2 had more significant effects in both LW (warming) and SW (cooling) and their net effect is about the same as the observation estimates. The SCM cloud type 7 had too strong cooling effect than the observations. We have shown that looking at the CRFs of different cloud types provides more information about the models' performance than only examining the CRF by all clouds. The errors in the LW and SW CRFs for a certain cloud type could be caused by many possible reasons, such as the defects in the simulated cloud amount, the incorrect timing that the clouds presented, as well as the weaknesses in the temperatures (vertical locations) and optical properties of the clouds. To reveal the possible reasons causing the weaknesses found in the simulated CRFs, we examined the overcast CRFs and the cloud amount of each cloud type.

5.2 Overcast Cloud Radiative Forcings

The overcast CRF of a cloud type is the CRF that the cloud type would have if it covered the whole sky, i.e., the cloud amount of that type is one. By definition, the overcast CRF is mainly determined by cloud-top temperature/pressure in LW and cloud optical depth in SW, and the impacts of cloud amount are excluded.

A. Overcast LW CRF

The overcast LW CRFs of the eight cloud types estimated from the satellite data and the two simulations averaged over the 14-day subperiods A, B, and C are shown in Figure 6. It is clear that the CRM overcast LW CRFs are almost the same as those observed, except they are about 10 Wm^{-2} larger for type 3. All three datasets show the dominant effects of the thick high-top clouds (type 4). Compared to the satellite observation, the overcast LW CRFs of the SCM's cloud types 2, 3, and 4 (high-top clouds with optical depth greater than 1.3) were about 30 Wm^{-2} smaller and that of its thin middle-top clouds (type 5) was about 30 Wm^{-2} larger. We calculated the mean, standard deviation, mode, and median of the frequency distribution of cloud-top pressure for each cloud type using the observational data, and the CRM and SCM results (Table 2). The CRM cloud types 2, 3, 4, 6 and 7 seems to have tops located lower than the satellite observations. This infers that their overcast LW CRFs could be lesser than the observations. However, their overcast LW CRFs (Figure 6) are about the same as the observations.

The reason is that the air temperatures were underestimated in the CRM simulation compared with the sounding data. The CRM underestimated the temperature by about 3°K at 600 to 200 mb and by 2°K at 800 to 600 mb, which could contribute to about 10 Wm^{-2} more overcast LW CRF.

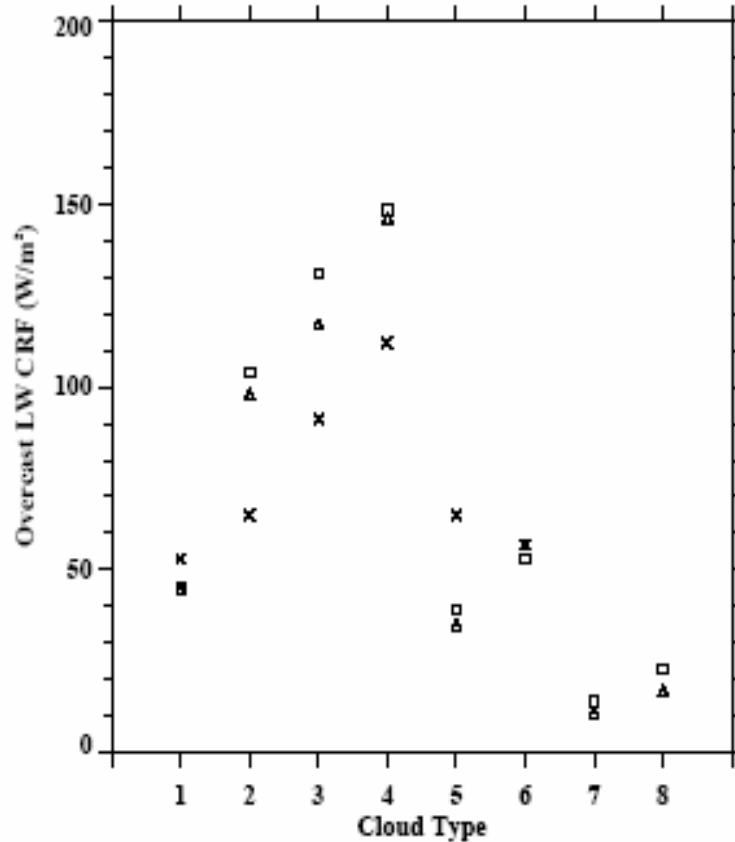


Figure 6. The overcast LW CRFs of the eight cloud types from the satellite observation (triangles), the CRM (squares) and the SCM (crosses) simulations during the 14-day subperiods A, B, and C.

The SCM cloud type 4 had tops at lower heights and warmer temperatures than the satellite data and this could contribute to its lesser overcast LW CRF. The lower overcast LW CRFs of the SCM cloud types 2 and 3 can hardly be explained by their cloud-top pressure distributions indicating other factors influencing overcast LW CRFs. The SCM cloud type 3 had more small values of optical depth than the observation, as will be shown later in this section. The smaller cloud optical depth could decrease its overcast LW CRF due to the transmission of surface radiation through the cloud layers. At the tops of the cloud types 2, 3, and 4 (200 to 250 mb, Table 2) the SCM temperatures are about 6°K warmer than the sounding data, which could contribute to about 15 Wm⁻² lesser overcast LW CRF, i.e. about half of the differences shown in Figure 6. The Figure 1 in Luo et al. (2004) shows the temperature biases for the CRM and SCM. The SCM cloud types 5 had variations (standard deviations) of cloud-top pressure that were too small. However, their tops are not higher than the observations and the CRM so that it is not clear why they had too strong overcast LW CRF (Figure 6).

Table 2. The means, standard deviations, modes, and medians of the frequency distributions of cloud-top pressure during the 14-day ABC subperiods from the satellite data, and the CRM and SCM simulations.

cloud types	mean	std. dev.	mode	median
	Obs: CRM : SCM	Obs : CRM : SCM	Obs: CRM : SCM	Obs: CRM : SCM
1	205 : 200 : 134	86 : 89 : 77	139 : 109 : 89	168 : 173 : 100
2	238 : 249 : 223	77 : 68 : 75	189 : 234 : 214	211 : 252 : 206
3	262 : 279 : 264	69 : 56 : 62	213 : 275 : 241	244 : 282 : 253
4	220 : 256 : 260	67 : 59 : 49	191 : 218 : 242	201 : 252 : 252
5	553 : 521 : 557	70 : 69 : 25	452 : 461 : 550	548 : 520 : 553
6	534 : 564 : N/A	64 : 68 : N/A	452 : 586 : N/A	523 : 556 : N/A
7	794 : 782 : 871	72 : 52 : 16	786 : 835 : 862	742 : 794 : 864
8	761 : 742 : N/A	49 : 43 : N/A	767 : 710 : N/A	759 : 731 : N/A

B. Overcast SW CRF

For the overcast SW CRFs, we compared the daytime portion (0800 to 1700 local time) averages during the subperiods A, B, and C (Figure 7). Data at twilight were excluded from the averaging on purpose due to larger uncertainties in the satellite retrievals around twilight. The CRM results are about the same as the observation except that the absolute value for its thick low-top clouds (type 8) was about 60 Wm^{-2} smaller. Except for the very thin high-top clouds (type 1) the overcast SW CRFs of the SCM's cloud types were significantly different from the satellite observations. In the SCM simulation, the overcast SW CRFs were too small for the high-top cloud types (particularly type 4), while they were too large for thin clouds with middle-and low-tops (types 5 and 7). No cloud types 6 and 8 (thick clouds with middle-and low-tops, respectively) were simulated by the SCM during the averaging periods. The overcast SW CRF of a certain cloud type is mainly determined by the cloud optical depth because optically thicker clouds reflect more solar radiation (i.e. have larger SW albedo) than thinner ones. However, the diurnal cycle variations of solar zenith angle (θ) play a role, also, as suggested by Eqs. (3) and (4). For example, clouds present at noon have larger overcast SW CRFs than they would have in the early morning or late afternoon, and night time clouds have no effects on SW radiation. To separate this effect of θ from that due to the cloud optical depth variations, we used a constant θ , equal to the daytime average value, but with the solar constant reduced by the day fraction, to diagnose the overcast SW CRFs. We call this method "constSZA". The overcast SW CRFs obtained using this method (Figure 8) are about half of their counterparts in Figure 7. This is because a diurnally average solar radiation was used in the "constSZA" method and the values shown in Figures 7 and 8 are daytime averages. The differences between the models and the observations shown in Figure 8 should be multiplied by a factor of about two when compared with those shown in Figure 7. The differences shown in Figure 8 between the CRM and the observations are larger for optically thin than thick cloud

types (except type 8). This indicates that the distributions of cloud optical depth in the CRM are simulated better for thick clouds than for thin clouds. The CRM errors for thin clouds in Figure 8 (constSZA), when multiplied by two, are larger than those in Figure 7. We infer from this that the errors in overcast LW CRFs of thin clouds caused by wrong present times partly cancelled out those due to unrealistic optical depth distribution. Under the same constant solar zenith angle, the SCM cloud types 2, 3, and 4 would have closer overcast SW CRFs to the observation than they had under diurnally varying θ . However, for the cloud types 1, 4, 5, and 7, the SCM values would still be significantly different from the observation. This suggests that (a) cloud types 1, 4, 5, and 7 had different optical property distributions from the observation so that even when they were simulated at the correct times, their overcast SW CRF would not be correct; (b) the SCM cloud types 2 and 3 had more reasonable distributions of optical properties than other cloud types, but the SCM did not always simulate their presence at the correct times.

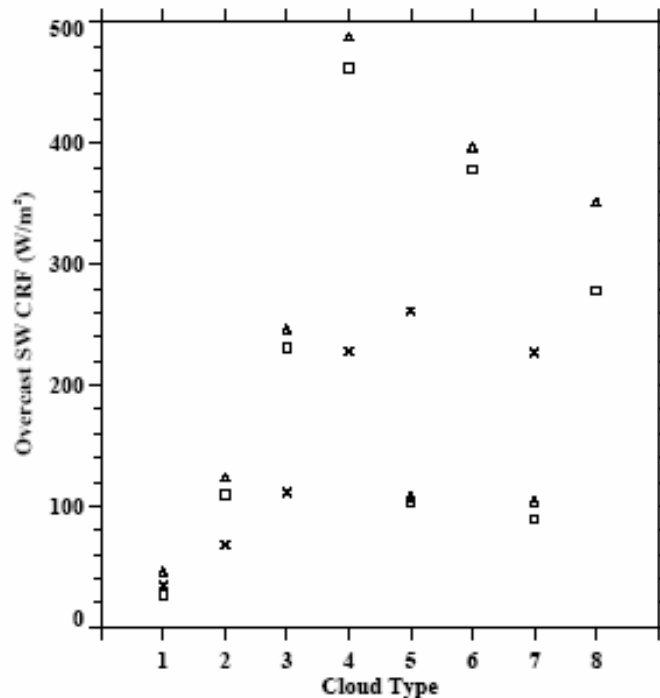


Figure 7. The overcast SW CRFs of the eight cloud types from the satellite observation (triangles), the CRM (squares) and the SCM (crosses) simulations during the 14-day subperiods A, B, and C.

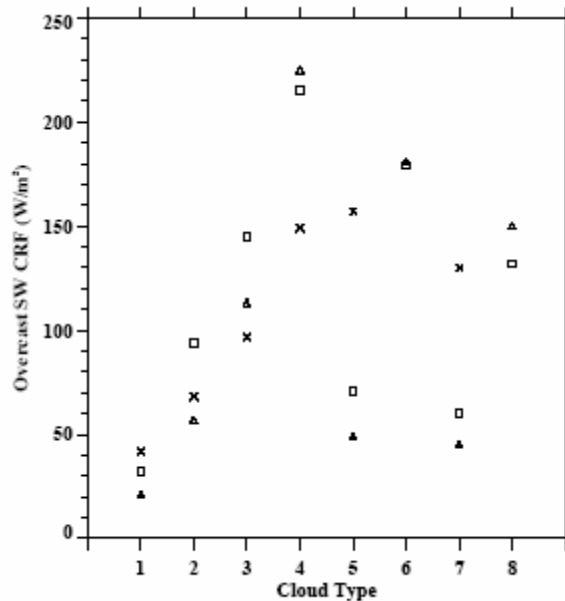


Figure 8. Similar to Figure 7, but the overcast SW CRFs were obtained using a constant solar zenith angle, equal to the daytime average value, with the solar constant reduced by the day fraction.

The normalized frequency distributions of cloud optical depth (τ) for each cloud type τ during the daytime, except for types 6 and 8 since the SCM did not simulate any of them during the daytime portion of the 14-day subperiods, are shown in Figure 9. Compared to the satellite data, the distributions of τ for very thin high-top clouds and thin middle-top clouds (types 1 and 5) in the SCM were skewed towards larger τ . For the thick high-top clouds (type 4), the optical depths produced by the SCM were too small and their distribution was too narrow. These can explain why the overcast SW CRFs produced by the SCM are too large for types 1 and 5, and too small for type 4 (Figure 8). The τ distribution of cloud type 7 (thin low-top clouds) was too narrow and lack large values. This is puzzling, because unrealistically small values of τ would result in overcast SW CRFs that are too weak, which is opposite to what is shown in Figure 8.

5.3 Cloud Type Amounts

Cloud amount influences CRF for obvious reasons. The production of correct cloud optical properties and temperatures does not mean that the correct CRFs are produced, unless the cloud occurrence (frequency and timing) is also correctly simulated. Using the 3 hr time-series of the eight cloud type amounts during the subperiods A, B, and C, we computed the temporal correlations between the simulations and the satellite observation, as well as the simulated standard deviations normalized by those from the observation. The results are provided by Table 3. The CRM underestimated the occurrences of high-top clouds (types 2, 3, and 4) and of thin clouds with middle- and high-tops (types 5 and 7) compared to the satellite data. This contributed to lesser CRFs of these cloud types as shown in Figures 4 and 5. Too large a fall-speed of large ice crystals (“snow”) could contribute to lower cirrus cloud amount in the CRM. The low vertical resolution in the middle and upper troposphere of the simulation (600 to 800 m) and of the large-scale forcing data (50 mb) could miss some shallow clouds.

Detrainment source of cloud ice could be underestimated due to too much graupel formation in simulation. The underestimation of the CRM's thin clouds at mid-and low-level could be partly due to too low horizontal resolution used (2 km), and partly because of neglecting the subgrid-scale condensation.

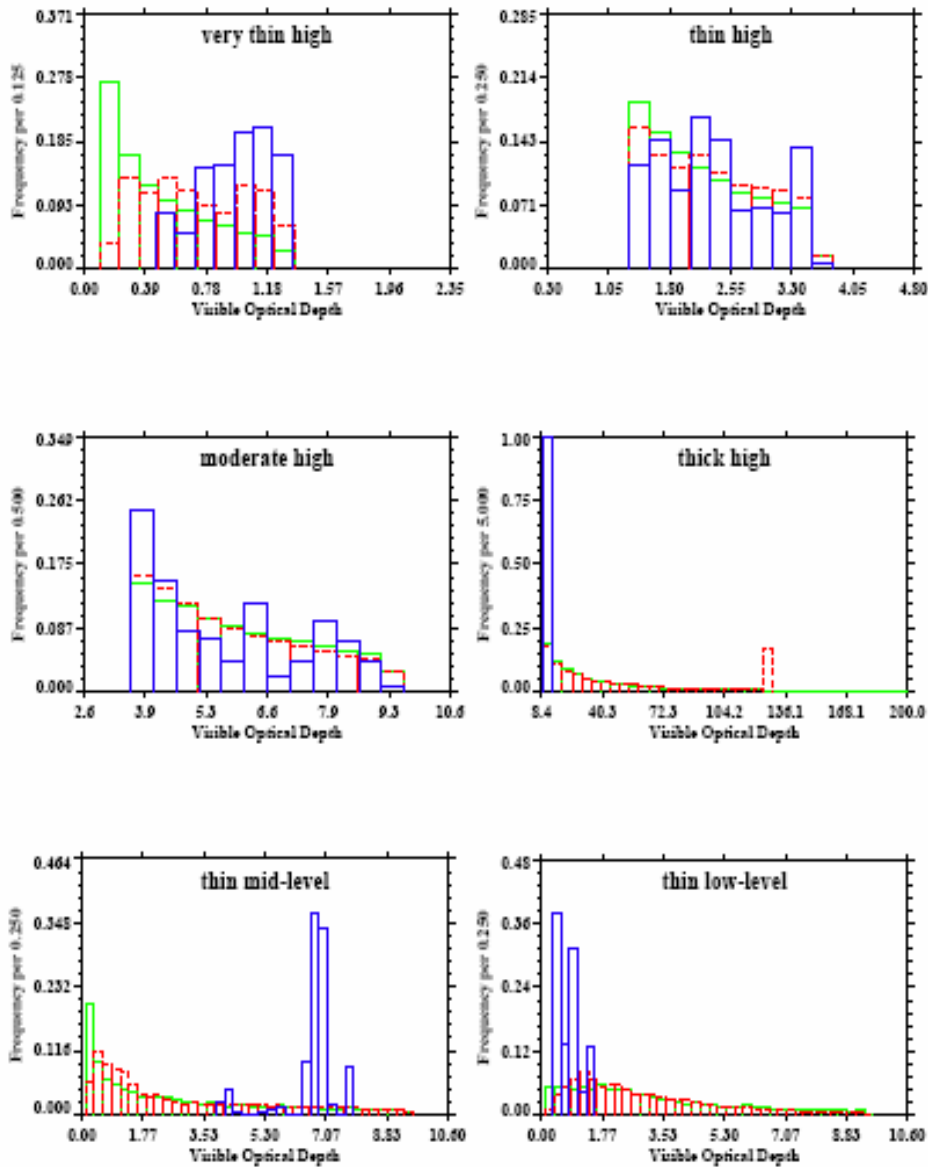


Figure 9. The frequency distributions of cloud optical depth for the six cloud types from the satellite observation (red), the CRM (green) and the SCM (blue) simulations during the 14-day subperiods A, B, and C. The panels from left to right at the top are cloud types 1 and 2, at the middle are cloud types 3 and 4, and at the bottom are cloud types 5 and 7.

Table 3. Statistics of 3 hourly cloud type amounts during the 14-day ABC subperiods. The first column is the mean cloud amounts in percentage. The second column is the differences of the mean cloud amounts between the simulations and the observation. The third column represent the CRM and SCM's standard deviations normalized by those of the observation. The forth column is the temporal correlation coefficients of the two simulations, respectively, with the observation.

cloud types	mean (%)	mean error (%)	std. dev.	correlation coefficient
	Obs: CRM : SCM	CRM : SCM	CRM : SCM	CRM : SCM
1	11 : 11 : 7	0 : -4	0.75 : 0.86	0.18 : 0.04
2	8 : 5 : 19	-3 : 11	0.74 : 2.05	0.36 : 0.43
3	7 : 4 : 10	-3 : 3	0.73 : 2.07	0.47 : 0.37
4	10 : 9 : 3	-1 : -7	0.81 : 0.76	0.64 : 0.48
5	5 : 2 : 1	-3 : -4	0.61 : 1.46	0.41 : 0.06
6	2 : 2 : 0	0 : -2	0.90 : N/A	0.61 : N/A
7	4 : 1 : 8	-3 : 4	0.33 : 4.54	0.47 : -0.06
8	1 : 1 : 0	0 : -1	1.13 : N/A	0.27 : N/A

The SCM overestimated the occurrences of thin to moderate high-top clouds (types 2 and 3, by 0.11 and 0.03 respectively) and underestimated that of thick high-top clouds (type 4, by -0.07), which contributed to CRFs that were too strong and too weak, respectively (Figures 4 and 5). The radiative effects of convective clouds are neglected in the SCM simulation and our analysis. Deep convective clouds, if included in the SCM analysis, would be classified as cloud type 4. This could be one reason for the SCM's underestimation of cloud type 4's amount. Neglecting the radiative effects of convective clouds in a general circulation model is probably reasonable when averaged over a long period (one month) and a large area (global). However, it may be necessary to include their effects if one focuses on the local CRFs during short periods when convective activity frequently happens as in this case. Another reason is closely related to the way that cumulus detrainment is represented in the SCM. In the SCM, cloud condensate is detrained into a single model layer at a time and spreads to entire grid area within one time step, i.e. cloud fraction at the detrainment layer is one. These detrainment-formed clouds have the same thickness (the SCM's grid vertical interval). In reality (and the CRM), detrainment occurs over thicker layers at a time. The thicknesses of the detrainment-associated clouds decrease with the distance away from the convective source, i.e., there is a wider range of distribution of cloud physical and optical thickness, i.e., cloud types. The SCM's inability to represent multiple cloud types formed by detrainment from cumulus tops could result in underestimation/overestimation of the amount for thick/thinner high-top clouds. One major conclusion from the recent model intercomparison project organized by the ARM Cloud Parameterization and Modeling Working (CPM) Group is that the climate models overestimate optically thick (τ greater than 23) clouds at all altitudes (Zhang et al. 2004). All of the 10 General circulation models participated in this model intercomparison project use one of the mass flux-form schemes to parameterize the deep convection (Tiedtke 1989, Gregory and Rowntree 1990, Gregory and Allen 1991, Emanuel 1991, Moorthi and Suarez 1992, Del Genio and Yao 1993, Zhang and

McFarlane 1995). Detrainment of condensate at multiple layers is included as a source term for the prediction of stratiform cloud condensate in these convection parameterization schemes. We suspect the overestimation of thick clouds is closely related to the parameterization of cloud condensate detrainment.

The CRM simulated temporal correlations with the observation were higher for all cloud types except type 2 than the SCM. Both the CRM and the SCM results show that thick high-top clouds had the best correlations with the observation among all cloud types (CRM 0.64 and SCM 0.48), while very thin high-top clouds had the worst correlations (CRM 0.18 and SCM 0.04). This suggests that the two models could simulate the generation of deep convective clouds (and the associated thick anvil clouds) with some success (though improvement is desired). However they had more difficulties in representing the formation and evolution of thinner high-top clouds. The SCM had very poor correlations with the observation for cloud type 5 (0.06) and 7 (-0.06), indicating that the representation of the mechanisms generating/maintaining the middle-and low-top clouds in the SCM needs improvement. The SCM simulated too much temporal variability in the occurrences of cloud types 2, 3, and 5.

5.4 Mean and Root-Mean-Square Errors

We list the mean values over the 14-day subperiods of cloud amounts, CRFs, and overcast CRFs by all clouds from the Minnis data, the CRM and SCM simulation results in the first 3 columns of Table 4. The 4th and 5th columns of Table 4 contain the differences between the averages from the simulations and the Minnis data. The 6th and 7th columns provide the root-mean-square errors by cloud types in both the CRM and the SCM simulations. Times near twilight were excluded in the averaging for daytime and night time cloud amounts, but included in the all day (24 hr) averaging. The SW overcast CRFs are daytime averages. Compared to the satellite observation, the SCM had the same cloud amount when averaged over the 14-day subperiods because it overestimated the cloud occurrence in daytime while underestimated it during night. The CRM simulation underestimated the cloud occurrence in both daytime and night time. Based on the mean errors only, one may conclude that the SCM did a better job in simulating the cloud occurrence than the CRM did. However, the SCM rms errors by cloud types were about twice as large as those from the CRM in both day and night. This suggests that the errors for different cloud types cancelled one another out in the SCM simulation, and the CRM actually performed better than the SCM.

The mean errors in the net CRF were 5 (CRM) and 9 (SCM) Wm^{-2} . The rms error of net CRF by the SCM cloud types was about twice of the CRM's (11 vs 5 Wm^{-2}). The SCM had about the same mean error in LW CRF as the CRM (-8 vs -7 Wm^{-2}), and larger mean error in SW CRF (17 vs 12 Wm^{-2}). However, its rms errors in LW and SW CRFs by cloud types were about three times of the CRM's. This shows, again, that the CRM simulated the radiative effects of various cloud types better than the SCM did and that mean errors in CRFs by all clouds can provide very limited, sometimes even misleading, information about a model's clouds.

TABLE 4. Means, mean errors, and root-mean-square errors for cloud amount, cloud radiative forcing (CRF), and overcast CRF. The first 3 columns contain the mean values from the satellite observation, and the CRM and SCM simulations, respectively, by all clouds during the 14-day subperiods A, B, and C. The 4th and 5th columns are the mean errors by all clouds in the CRM and SCM simulations, respectively. The 6th and 7th column are the rms errors by cloud types. For cloud amounts, results during all day (24 hr), daytime, and night time are provided. For overcast SW CRFs, the values shown are daytime averages. The last row contains the overcast SW CRFs diagnosed using a constant solar zenith angle, equal to daytime average value, but with the solar constant reduced by the day fraction.

		mean			mean error		rms error	
		obs	CRM	SCM	CRM	SCM	CRM	SCM
cloud amount (%)	24 hr	48	35	48	-13	0	6	15
	Day	42	34	51	-8	0	11	19
	Night	52	34	49	-18	-3	12	20
CRF (W m-2)	net	-5	0	4	5	9	5	11
	LW	38	31	31	-7	-8	4	13
	SW	-43	-31	-27	12	17	8	22
overcast CRF (W m-2)	LW	66	70	57	4	-9	18	62
	SW	186	170	155	-16	-31	41	249
	SW_sza	85	103	107	18	22	58	160

6. Summary and Discussions

The TOA radiative effects and occurrence frequencies of various cloud types in 29-day simulations performed by a SCM and a CRM using large-scale forcing data from the ARM variational analysis at the SGP site were diagnosed. The results were compared with those estimated from the pixel-level satellite observations. During the simulation period, most clouds were observed by both the satellite and the millimeter cloud radar to have their tops at high-level (above 440 mb). We grouped the clouds into eight types defined by their total optical depth and cloud top pressure with four at the high-level and two at the mid-and low-levels, respectively. For this particular case, the CRM is found to simulate CRFs and occurrence frequencies of the eight cloud types much realistic than the SCM, as measured by the rms errors caused by cloud types. The SCM quantity that agrees most closely with the observations and CRM is total net CRF, a quantity that is tuned in General circulation models to obtain a global TOA energy balance (but not a local balance as in this case). However, when the SCM's net CRF is decomposed into cloud type components, it is evident that the total net CRF is a result of compensating errors in the CRFs of individual cloud types: the high clouds have too great a warming effect, while the low clouds have too great a cooling effect.

We found that the SCM simulated too few occurrences of thick (τ greater than 9.4) high-top clouds (type 4), and this cloud type had a optical depth distribution that is too narrow lacking large values of τ . As a result, these thick high-level clouds had a net warming effect at the TOA in the SCM as opposed to the observation and the CRM which show a net cooling effect. We suspect that the too few occurrence of the SCM's thick high-top clouds is partly due to the unrealistic representation of detrainment of cloud

condensate from the tops of cumulus towers, and partly because of neglecting convective clouds in radiation calculation. The SCM overestimated the occurrence of thin (τ between 1.3 and 3.6) cirrus clouds (type 2) and thin (τ less than 9.4) middle-top clouds (type 7), and hence overestimated their radiative effects. Both the SCM and the CRM simulated the occurrences of thick high-top clouds which are correlated better with the observation than the simulated thinner high-top clouds. The major weakness found in the CRM simulation was the underestimation of the occurrences for high-top clouds and thin clouds with middle-and low-top, though the CRM was found to simulate CRFs and overcast CRFs comparable to the observation. Possible reasons are discussed in Section 5.3. We have not explored the physical processes which are responsible for the errors found in the models, though it is essential to finally improve the models' performance. The SCM and CRM are used as examples to demonstrate the usefulness of the new evaluation method, which is the major objective of this study.

Clouds influence the radiation budget through their greenhouse (warming) and albedo (cooling) effects. The former effect is mainly determined by the cloud-top temperature, the latter by cloud optical depth, while cloud occurrence frequency (amount and timing) has an impact on both LW and SW. As demonstrated by other studies and this study, the net radiative effects by different cloud types are not the same due to the differences in their top temperatures, optical depths, and cloud occurrence frequencies. The formation and evolution of cloud types is related to various physical processes. Some processes may be more responsible for certain cloud types than other processes. Errors due to certain cloud types probably compensate those by other cloud types resulting in small net errors. As found very recently by the Cloud Parameterization and Modeling Working Group within the ARM program, 10 General circulation models simulated incorrect cloud type amounts: overestimated the occurrence of thick clouds (τ greater than 23) and underestimated that of thinner clouds. This means that the General circulation models simulated distributions of cloud types are different from those observed. However, they simulated better CRFs at the TOA and their seasonal variations than cloud types due to compensatory errors (Zhang et al. 2004). In order to essentially improve the representation of clouds and their radiative effects in a model (CRM, SCM/general circulation model), we cannot rely on the compensation of the errors. Efforts must be made toward an improvement for each cloud type. Therefore, it is necessary to evaluate the model in terms of cloud types, in addition to the averages by all cloud types. The most problematic cloud types can be revealed using this method.

The most problematic cloud types found in a model would be the modeler's target for further study. The efforts should then be made toward revealing reasons for the weaknesses in simulating those cloud types. One can integrate this method, i.e. examining models' cloud types using km-scale observations, with the compositing techniques and case studies. By compositing observations and model results using some criteria that describe the main mechanisms in cloud generation, maintenance, and/or decay, a first link to the possible reasons for model problems is established. Comparing simulations for real cases performed by SCMs and CRMs can probably identify the SCM's problems. In addition, idealized simulations using CRMs and/or SCMs may be set up specially for better understanding some processes and/or for revealing errors of their representation in models.

Acknowledgements

This research was supported by the Environmental Sciences Division of the U.S. Department of Energy (DOE) as part of the Atmospheric Radiation Measurement program, under Grant DE-FG03-94ER61769.

The authors thank Patrick Minnis' group at the NASA Langley Research Center for providing their cloud products.

References

Ackerman, Thomas, and Gerry Stokes. 2003: The Atmospheric Radiation Measurement Program. *Physics Today*, **56**, 38 - 45.

Cess, R. D., and coauthors, 1996: Cloud feedback in atmospheric general circulation models: An update. *J. Geophys. Res.*, **101**, 12,791-12,794.

Chaboureau, J., P. Bechtold, 2002: A simple cloud parameterization derived from cloud resolving model data: Diagnostic and prognostic applications. *J. Atmos. Sci.*, **59**, 2362-2372.

Fu, Q., and K. N. Liou, 1992: On the correlated k-distribution method for radiative transfer in nonhomogeneous atmospheres. *J. Atmos. Sci.*, **49**, 2139-2156.

--, and --, 1993: Parameterization of the radiative properties of clouds. *J. Atmos. Sci.*, **50**, 2008-2025.

Grabowski, W. W., 2001: Coupling cloud processes with the large-scale dynamics using the cloud-resolving convection parameterization (CRCP). *J. Atmos. Sci.*, **58**, 978-997.

Hu, Y. X., and K. Stamnes, 1993: An accurate parameterization of the radiative properties of water clouds Suitable for use in climate models. *J. Climate*, **6**, 728-742.

IPCC, 2001: Intergovernmental Panel on Climate Change, *Climate Change 2001*, Third Assessment Report of the IPCC. The Scientific Basis. A contribution of Working Group I. Cambridge University Press. Jakob, C., 2003: An improved strategy for the evaluation of cloud parameterizations in GCMs. *Bull. Amer. Meteor. Soc.*, **84**, 1387-1401.

Khairoutdinov, M. F., and D. A. Randall, 2001: A cloud resolving model as a cloud parameterization in the NCAR Community Climate System Model: Preliminary results. *Geophys. Res. Lett.*, **28**, 3617-3620.

--, --, and C. Demott, 2003: Simulations of the atmospheric general circulation using a cloud-resolving model as a super-parameterization of physical processes. Submitted to *J. Atmos. Sci.*.

Khayer, M. M., A. D. Rapp, D. R. Doelling, M. L. Nordeen, P. Minnis, W. L. Smith, L. Nguyen, and Q.-L. Min, 2002: Evaluation of a 5-year cloud and radiative property dataset derived from GOES-8 data over the Southern Great Plains. *Proc. 12th Atmospheric Radiation Measurement (ARM) Science Team Meeting*, St. Petersburg, Florida, Atmospheric Radiation Measurement Program. [Available at http://www.arm.gov/docs/documents/technical/conf_0204/khayer-mm.pdf]

Klein, S. A., and C. Jakob, 1999: Validation and sensitivities of frontal clouds simulated by the ECMWF model. *Mon. Wea. Rev.*, **127**, 2514-2531.

Kohler, M., 1999: Explicit prediction of ice clouds in general circulation models. Ph.D. dissertation, University of California, Los Angeles, 167 pp. Available from Department of Atmospheric Sciences, University of California, 405 Hilgard Avenue, Los Angeles, CA 90095.

Krueger, S. K., 1988: Numerical simulation of tropical cumulus clouds and their interaction with the subcloud layer. *J. Atmos. Sci.*, **45**, 2221-2250.

--, Q. Fu, K. N. Liou, and H-N. S. Chin, 1995a: Improvements of an ice-phase microphysics parameterization for use in numerical simulations of tropical convection. *J. Applied Meteor.*, **34**, 281-287.

--, G. T. McLean, and Q. Fu, 1995b: Numerical simulation of the stratus-to-cumulus transition in the subtropical marine boundary layer. Part I: Boundary-layer structure. *J. Atmos. Sci.*, **52**, 2839-2850.

--, G. T. McLean, and Q. Fu, 1995c: Numerical simulation of the stratus-to-cumulus transition in the subtropical marine boundary layer. Part II: Boundary-layer circulation. *J. Atmos. Sci.*, **52**, 2851-2868.

Luo, Y.-L., S. K. Krueger, G. G. Mace, and K.-M. Xu, 2003: Cirrus cloud statistics from a cloud-resolving model simulation compared to cloud radar observations. *J. Atmos. Sci.*, **60**, 510-525.

--, --, and S. Moorthi, 2004: Cloud Properties Simulated by a Single-Column Model. Part 1: Comparison to Cloud Radar Observations of Cirrus Clouds. Conditionally accepted by *JAS*.

--, --, 2004: Cloud Properties Simulated by a Single-Column Model. Part 2: Evaluation of detrainment and microphysics using a cloud resolving model. To be submitted.

Mace, G. G., E. E. Clothiaux, and T. P. Ackerman, 2001: The composite characteristics of cirrus clouds; bulk properties revealed by one year of continuous cloud radar data. *J. Climate*, **14**, 2185-2203.

Minnis, P., and W. L. Smith, Jr., 1998: Cloud and radiative fields derived from GOES-8 during SUCCESS and the ARM-UAV Spring 1996 Flight Series. *Geophys. Res. Ltrs.*, **25**, 11131116.

--, D. P. Garber, D. F. Young, R. F. Arduini, and Y. Takano, 1998: Parameterizations of reflectance and effective emittance for satellite remote sensing of cloud properties. *J. Atmos. Sci.*, **55**, 3313-3339.

--, D. P. Kratz, J. A. Coakley, Jr., M. D. King, D. Garber, P. Heck, S. Mayor, D. F. Young, and R. Arduini, 1995: Cloud Optical Property Retrieval (Subsystem 4.3). "Clouds and the Earth's Radiant Energy System (CERES) algorithm theoretical basis document, Volume III: Cloud analyses and radiance inversions (Subsystem 4)", NASA Tech. Rep. RP 1376, 135-176.

Moorthi, S., H.-L. Pan, and P. Caplan, 2001: Changes to the 2001 NCEP operational MRV/AVN global analysis/forecast system, *NWS Technical Procedures Bulletin*, 484, pp14. [Available at <http://www.nws.noaa.gov/om/tpb/484.htm>]

Norris, J. R., and C. P. Weaver, 2001: Improved Techniques for Evaluating GCM Cloudiness Applied to the NCAR CCM3. *J. of Climate.*, **14**, 2540-2550.

- Pan, H.-L., and W.-S. Wu, 1995: Implementing a mass flux convection parameterization package for the NMC medium-range forecast model. National Meteorological Center, Office Note 409, 40 pp.
- Randall, D., K.-M. Xu, R. J. C. Somerville, and S. Iacobellis, 1996: Single-column models and cloud ensemble models as links between observations and climate models. *J. of Climate.*, **9**, 1683-1697.
- Randall, D., and coauthors, 2003: Confronting models with data. *Bull. Amer. Meteor. Soc.*, **84**, 455-469.
- Rossow, W. B., and R. A. Schiffer, 1991: ISCCP cloud data products. *Bull. Amer. Meteor. Soc.*, **72**, 2-20.
- , and --, 1999: Advances in understanding clouds from ISCCP. *Bull. Amer. Meteor. Soc.*, **80**, 2261-2289.
- , A. W. Walker, D. Beuschel, and M. Roiter, 1996: International Satellite Cloud Climatology Project (ISCCP) description of new cloud datasets. WMO/TD 737, World Climate Research Programme (ICSU and WMO), 115 pp.
- Senior, C. A., and J. F. B. Mitchell, 1993: Carbon dioxide and climate: the impact of cloud parameterization. *J. of Climate*, **6**, 393-418.
- Stokes, G. M. and S. E. Schwartz, 1994: The Atmospheric Radiation Measurement (ARM) Program: Programmatic background and design of the Cloud and Radiation Testbed. *Bull. Amer. Meteor. Soc.*, **75**, 1201-1221.
- Tselioudis, G., Y. Zhang, and W. B. Rossow, 2000: Cloud and radiation variations associated with northern midlatitude low and high sea level pressure regimes. *J. Climate*, **13**, 312-327.
- Weare, B. C., and AMIP modeling groups, 1996: Evaluation of the vertical structure of zonally averaged cloudiness and its variability in the Atmospheric Model Intercomparison Project. *J. Climate*, **9**, 3419-3431.
- Wielicki, B. A., B. R. Barkstrom, E. F. Harrison, R. B. Lee III, G. L. Smith, and J. E. Cooper, 1996: Clouds and the Earth's Radiant Energy System (CERES): An Earth Observing System Experiment. *Bull. Amer. Meteor. Soc.*, **77**, 853-868.
- Xie, S. C., and coauthors, 2002: Intercomparison and evaluation of cumulus parameterizations under summertime midlatitude continental conditions. *Q. J. R. Meteorol. Soc.*, **128**, 1095-1135.
- Xu, K.-M., and D. Randall, 1995: Impact of interactive radiative transfer on the macroscopic behavior of cumulus ensembles. Part I: Radiation parameterization and sensitivity test. *J. Atmos. Sci.*, **52**, 785-799.

--., T. Wong, B. A. Wielicki, D. A. Randall, L. Parker, and Z. A. Eitzen, 2004: Statistical analyses of satellite cloud object data for large ensemble evaluation of cloud models. Part I: Methodology and preliminary results. Submitted to *J. Geophys. Res.*.

Young, D. F., P. Minnis, W. L. Smith Jr., and D. P. Garber, 1997: A four-channel method for deriving cloud radiative properties from meteorological satellite data. *IRS '96: Current Problems in Atmospheric Radiation*, W. L. Smith and K. Stamnes, Eds., Deepak, 612615.

Zhang, M. H., and J. L. Lin, 1997: Constrained variational analysis of sounding data based on column-integrated budgets of mass, heat, moisture, and momentum: approach and application to ARM measurements. *J. Atmos. Sci.*, **54**, 1503-1524.

--., --., R. T. Cederwall, J. J. Yio, and S. C. Xie, 2001: Objective analysis of ARM IOP data: method and sensitivity. *Mon. Wea. Rev.*, **129**, 295-311.

--., and coauthors, 2004: Comparing clouds and their seasonal variations in 10 atmospheric General Circulation Models with satellite measurements. Submitted to *J. Geophys. Res.*.